MOLECULAR IMAGING AND BIOLOGY

Published Online: 28 August 2010

Mol Imaging Biol (2011) 13:679–694
DOI: 10.1007/s11307-010-0403-0

RESEARCH ARTICLE

In Vivo Cellular MRI of Dendritic Cell Migration Using Micrometer-Sized Iron Oxide (MPIO) Particles

Roja Rohani,[1,2] Sonali N. de Chickera,[3,4] Christy Willert,[4] Yuhua Chen,[2] Gregory A. Dekaban,[4,5] Paula J. Foster[1,2]

[1]*Department of Medical Biophysics, University of Western Ontario, London, Ontario, Canada*
[2]*Imaging Research Laboratories, Robarts Research Institute, University of Western Ontario, London, Ontario, Canada*
[3]*Department of Anatomy and Cell Biology, University of Western Ontario, London, Ontario, Canada*
[4]*BioTherapeutics Research Laboratories, Robarts Research Institute, University of Western Ontario, London, Ontario, Canada*
[5]*Department of Microbiology and Immunology, Robarts Research Institute, University of Western Ontario, London, Ontario, Canada*

Abstract

Purpose: This study seeks to assess the use of labeling with micron-sized iron oxide (MPIO) particles for the detection and quantification of the migration of dendritic cells (DCs) using cellular magnetic resonance imaging (MRI).

Procedures: DCs were labeled with red fluorescent MPIO particles for detection by cellular MRI and a green fluorescent membrane dye (PKH67) for histological detection. MPIO-labeled DCs or unlabeled control DCs were injected into mice footpads at two doses (0.1×10^6 and 1×10^6). Images were acquired at 3 Tesla before DC injection and 2, 3, and 7 days post-DC injection.

Results: Labeling DCs with MPIO particles did not affect viability, but it did alter markers of DC activation and maturation. MRI and fluorescence microscopy allowed for the detection of MPIO-labeled DCs within the draining popliteal nodes after their injection into the footpad.

Conclusions: This paper presents the first report of the successful use of fluorescent MPIO particles to label and track DC migration.

Key words: MRI, Dendritic cells, Cancer, Immunotherapy, Iron oxide, Contrast agent, MPIO

Significance This paper is the first report of the successful use of micron-sized iron (MPIO) nanoparticles to track dendritic cells (DCs) migration with magnetic resonance imaging (MRI). We demonstrate that labeling DCs with MPIO does not affect viability of DCs and that cellular MRI can be used to reliably detect migration of MPIO-labeled DCs to the draining lymph nodes *in vivo* in the short term. The MPIO used to label DCs were also fluorescently tagged with Flash Red, and the DCs themselves were labeled with PKH67, a green intercalating membrane dye, which allowed for the direct detection of DCs and of MPIO particles and permitted careful comparisons between the MRI and fluorescence images.

Correspondence to: Paula J. Foster; *e-mail:* pfoster@imaging.robarts.ca

Introduction

The utilization of cells of the immune system to recognize and eliminate cancer cells is the primary goal behind cancer immunotherapy. Although promising, efforts to elicit anti-tumor immunity using standard vaccine approaches, which employ tumor cell extracts, killed tumor cells, or defined tumor-specific antigens, have not provided consistent and sufficiently efficacious results [1, 2]. Recently, the use of immune cells as adjuvants in cancer vaccines has shown promise and gained interest [3]. Perhaps the most

promising of the cell-based vaccines is the dendritic cell (DC)-based vaccine [4]. DCs are highly specialized antigen presenting cells, important for initiating and regulating primary immune responses. DCs in peripheral tissues are capable of taking up either foreign or self antigen (Ag), and in the presence of the necessary pro-inflammatory signals, they migrate to secondary lymphoid tissue. It is within the secondary lymphoid tissue, namely the lymph nodes, where DCs are capable of interacting with T and B cells to induce Ag-specific immune responses. Specifically, the ability of the DCs to present Ag to naive T cells, acting as an adjuvant, is a unique feature of this cell in comparison to other antigen presenting cells. Together, these features provide the basis upon which DCs are favored for their use in cell-based vaccine immunotherapies.

To date, results of clinical trials investigating DC-based cancer vaccines have been promising, demonstrating that they are safe and non-toxic. Compared to other cancer vaccine approaches, DC-based cancer vaccines show the highest objective response rate of around 10% and are capable of generating tumor-specific immune responses and reductions in metastasis [5–7]. Nevertheless, the majority of vaccinated patients do not respond, therefore, demonstrating that the overall efficacy of the DC-based cancer vaccine has yet to reach its full potential.

Improving DC-based vaccines requires the optimization of a variety of parameters, such as the state of DC maturation and the route of vaccine administration. Ultimately, the success of this immunotherapy depends on the efficient migration of DCs to secondary lymphoid organs. However, it was determined that following either subcutaneous or intradermal injection, only 0.01–3% of *ex vivo*-generated DCs migrated to target lymph nodes [8, 9]. Current conventional methods used to assess the *in vivo* migration of human DCs are highly invasive and require partial or full tissue biopsy. Certain image-based techniques, such as scintigraphy or positron emission tomography (PET), provide non-invasive imaging information with respect to DC trafficking in a sensitive and quantitative manner. However, neither scintigraphy nor PET is capable of providing detailed three-dimensional (3D) anatomical information, preventing accurate localization of DC *in vivo*. Furthermore, these techniques require the use of radioactive tracers with short half-lives, preventing their use in longitudinal studies. The ability to conduct long-term non-invasive tracking studies would provide research clinicians with important information in order to determine the optimal parameters of vaccine preparation and delivery, which results in the most effective DC migration to lymph nodes. Ultimately, effective DC migration can potentially lead to improved, anti-tumor immune responses *in vivo*. Consequently, there is a need for a non-invasive, sensitive imaging technique that permits the longitudinal tracking of *in vivo* DC migration in human patients.

Previously, it has been demonstrated that DCs labeled with superparamagnetic iron oxide (SPIO) nanoparticles were subsequently detected *in vivo* by magnetic resonance imaging (MRI) [10–15]. These other studies have shown that DCs can take up SPIO with minimal or no effect on viability or function. Other groups have reported the use of MRI to track the *in vivo* migration of SPIO-labeled DC (SPIO-DC) to draining lymph nodes in either mouse or human models [10, 12, 14, 15]. The MRI detection of SPIO-DC injected directly into the lymph nodes in patients has also been demonstrated [10]. While tracking DC migration is of importance, accurate quantification of the amount of migration to lymph nodes is of equal relevance since the quality and magnitude of an immune response is directly related to the number of antigen presenting DC in the lymph node. Although the direct quantification of negative signal contrast is limited, cellular MRI techniques do allow for highly sensitive detection of a very few to single cells [16, 17]. Our group has previously shown that the migration of SPIO-DC can be tracked in mice using a clinical scanner, and the MR data obtained was used to semi-quantify the amount of DC migration [12].

To date, all studies that have used iron contrast agents to label and track DC migration *in vivo* with MRI have used SPIO. In this study, we explore the use of micron-sized iron oxide (MPIO) particles. MPIO particles typically used for MRI are approximately 1 μm in diameter compared to SPIO nanoparticles, which range from 50 to 120 nm in diameter. As Shapiro *et al*. have shown, the area of signal loss in MR images increases with increasing iron content per particle [18]. The iron content per particle is also much greater for a single MPIO particle compared to a SPIO nanoparticle. Thus, labeling cells with MPIO would increase the possibility of detecting smaller numbers of labeled cells or cells with fewer particles in them. Many different cell types have been labeled with MPIO, including macrophages [19, 20], T cells [21], glioma cells [22], hematopoietic progenitor, and mesenchymal stem cells [23], all of which remained unaltered in terms of their functionality and viability.

Current clinical vaccine protocols of DC-based cancer immunotherapies require *ex vivo* preparation and stimulation of autologous patient DCs [24]. For this study, we used unstimulated bone marrow-derived DCs in order to elucidate any effects MPIO labeling itself might have on the DC phenotype and *in vivo* DC migration alone. We demonstrate the feasibility of labeling DCs with fluorophore-conjugated MPIO particles with no effect on their viability. However, MPIO labeling of DC does affect their phenotype compared to the unlabeled control. For the first time, we provide the results of tracking and quantifying the amount of MPIO-labeled DC migration *in vivo* in a mouse model using cellular MRI.

Materials and Methods

Animals

All animal protocols were accredited by the University of Western Ontario Animal Use Subcommittee and complied with the outlined guidelines of the Canadian Council on Animal Care. Six- to eight-

week-old C57BL/6 male mice were obtained from Charles River (Saint-Constant, Quebec) and housed in the Robarts Research Institute Barrier Facility until use.

Reagents

RPMI 1640 culture medium (Gibco, Burlington, ON) was supplemented with 10% Δfetal-bovine serum (Hyclone, Logan, USA), 5 mL penicillin–streptomycin, 5 mL L-glutamine, 5 mL MEM non-essential amino acids, 5 mL sodium pyruvate, 5 mL HEPES buffer solution, and 500 μL 2-mercaptoethanol (Invitrogen, Burlington, ON). Mouse GM-CSF and IL-4 were gifts from Scheling-Plough. MPIO particles were obtained from Bangs Laboratories Inc. (Fishers, IN, USA). The MPIO particles used for these experiments were 0.90 μm in diameter and conjugated to the Flash Red fluorophore (excitation/emission peaks, 660:690 nm). Anti-mouse CD11c, CD11b, MHCII, CD80, and CD40 fluorophore-conjugated antibodies were purchased from Becton, Dickinson and Company (BD; Mississauga, ON). Anti-mouse CD86, CD54, CCR7, and biotinylated CD36 and CD38 antibodies and secondary antibodies (streptavidin–phycoerythrin) were purchased from BioLegend (San Diego, CA, USA). Anti-mouse biotinylated PD-L1 and PD-L2 were purchased from eBioscience (San Diego, CA, USA). Isotype controls were purchased from the same companies.

Dendritic Cell Culture and MPIO Labeling

DCs were derived from the bone marrow (BM) of mouse femurs and tibias as previously described [12]. On day 4 of culture, the BM-derived DC were enriched by centrifugation over a 13.5% *w/v* Histodenz gradient as previously described [12]. DCs were then labeled by overnight incubation with 12.5 μg/mL MPIO (Bangs beads, Bangs Laboratories, Fisher, IN, USA).

MPIO-labeled DCs were washed three times with Hank's balance salt solution (HBSS, Invitrogen) containing 0.1% bovine serum albumin (BSA; EMD Chemicals, Darmstadt, Germany) to ensure removal of unincorporated contrast agent. Unlabeled DCs were used as the experimental control.

DC Viability Assays

The trypan blue exclusion assay was performed to determine the viability of MPIO-labeled and unlabeled control cells. The amount of apoptotic and necrotic cell death was also determined by staining DCs with 7-amino-actinomycin (7AAD; BD) and Annexin V (BD), and analysis was carried out using flow cytometry.

Detection of Iron in DC

To detect intracellular uptake of MPIO particles, MPIO-labeled DCs were collected following overnight culture, washed three times with buffer, and deposited onto glass microscope slides using a cytospin centrifuge. Cells were stained for iron with Perl's Prussian blue and counterstained with eosin. To determine the cellular iron content, inductively coupled plasma mass spectroscopy (ICP-MS, Varian 800 MS) was performed by Dr. R. Raina, Department of Chemistry and Biochemistry, and the Trace Analysis Facility, University of Regina, Regina, Saskatchewan, Canada. Cells contained within 500 μL phosphate-buffered saline (PBS) were digested with 2 mL of Ultrex II ultrapure concentrated nitric acid (JT Baker, Phillipsburg, NJ, USA) and heated until the volume was reduced to approximately 0.5–1 mL. The digestate, which contained no solids, was made to a final volume of 10 mL with 1% ultrapure nitric acid. Iron was determined using the ^{57}Fe isotope, and ^{45}Sc was used as the internal standard at 2 μg L^{-1} in all standards and samples. Varian ICP-MS Expert Software was used for data collection and analysis. The ^{57}Fe isotope has been shown previously to be free of interferences, and all reagent blank samples showed no detectable levels of Fe [25]. Untreated cells were used as a control in all cases.

Detection of Surface Antigens

Cells were collected from overnight cultures on day 5 and washed three times with HBSS+0.1% BSA to remove free MPIO particles. Cells were first blocked using 5% *v/v* of normal goat serum for 20 min. Cells were then stained accordingly with the required antibodies. CCR7 staining was carried out at 20°C (room temperature) for 20 min. Other antibody staining was carried out at 4°C (on ice) for at least 20 min. Flow cytometry was performed using a FACS Calibur (BD) and analyzed with CellQuest Pro software (BD).

Luminex Assays

Luminex® 10-Plex mouse cytokine panel (Invitrogen) was used to determine the cytokine profile of supernatants collected from DCs following overnight incubation with MPIO. Supernatants collected from DCs left unlabeled were used as the control. The mouse cytokines analyzed were IL-1β, IL-2, IL-4, IL-5, IL-6, IL-10, IL-12, IFN-γ, TNF, and GM-CSF. The protocol was carried out as per manufacturer's instructions. Samples were analyzed using a Luminex 200 System, and at least 400 bead events were collected for each analysis.

Labeling DC with PKH

DCs were collected from day 5 cultures and washed one time in PBS. PKH67 (a green intercalating membrane dye) was used according to manufacturer's instructions (Sigma-Aldrich). Cells were washed three times, re-counted, and re-suspended accordingly in PBS for their subsequent injection into mice.

Injection of DC into Mice

Before DC injection, mice were anesthetized with isofluorane (Forane, Baxter; 1% in 99% oxygen). DCs were adoptively transferred via subcutaneous injection into the hind footpads of C57BL/6 mice at doses of either 0.1×10^6 or 1×10^6. $PKH67^+$ MPIO-labeled DCs were administered into the left hind footpads, while PKH^+-unlabeled cells were used as the control and were administered to the contralateral footpads.

Cellular MRI

MRI was performed using a 3 Tesla (3 T) GE whole-body MR scanner (MR Signa® Excite™, GE Healthcare, Milwaukee, WI, USA) with a custom-built gradient coil (inner diameter=17.5 cm, maximum gradient strength=500 mT/m, and peak slew rate= 3,000 T/m/s) and a solenoid radiofrequency (RF) coil (4 cm in length and 3 cm in diameter). Mice were anesthetized using isofluorane (2% in oxygen) and maintained during scans (1.5% isofluorane in oxygen). Mice were placed on a custom-built plastic sled for secure positioning. All mice were scanned 2 days before DC injection, and then mice were scanned on day 2 (n=16) or on days 2, 3, and 7 post-injection (n=8).

All images were acquired using the 3D fast imaging employing steady-state acquisition (3D-FIESTA; GE Medical Systems, Milwaukee, WI, USA) pulse sequence. The imaging parameters were: repetition time = 4.2 ms, echo time = 2.1 ms, flip angle = 20º, receiver bandwidth = ±62.5 kHz, 200 µm isotropic resolution over a 6 cm field of view, and eight RF phase cycles. Acquisition time was 21 min.

MR Image Analysis

The volume of the popliteal lymph nodes, the signal void volume, and the fractional signal loss in the nodes were measured from MR images. Measurements were obtained using VGStudio Max 1.2 (Heidelberg, Germany) imaging software. Lymph node volumes and signal void volumes were measured as previously described [12]. Briefly, volumes calculated using manual segmentation of either the lymph node or signal void in each image slice, and then a threshold was set in order to accurately delineate the area of interest from surrounding image pixels.

Fractional signal loss was used to assess the amount of signal loss generated due to presence of MPIO-labeled DC. The following calculation was used to determine the fractional signal loss:

$$\Delta S/S = (S - S_{\text{void}})/S$$

where S_{void} is the minimum signal intensity value from the central voxels of the void observed in the left popliteal lymph node and S is the average signal intensity value from the contralateral lymph node that received unlabeled DCs.

Tissue Histology and Microscopy

After MRI, mice were euthanized by CO_2 inhalation and the popliteal lymph nodes were removed. Lymph nodes were fixed with 10% formaldehyde in PBS overnight, and tissue cryoprotection was performed by sequential incubation (24 h) in an increasing sucrose gradient (10%, 20%, and 30%). For sectioning, lymph nodes were embedded in optimal cutting temperature compound (Sakura Finetek, Torrance, CA) and snap frozen using dry ice. Sections were cut at a thickness of 16 µm and placed on glass plus slides (VWR, Mississauga, ON).

Digital images were collected using a Zeiss Axioimager fluorescence microscope equipped with a Qimaging Retiga Exi color video camera. The amount of $PKH67^{+}$ cells was determined using digital morphometry to measure the ratio of green fluorescence: area of interest (lymph node) as previously described [26] using ImageJ 1.42 software. The amount of Flash Red fluorescence was also measured using digital morphometry.

Statistical Analysis

Results of measurements are reported as the mean ± SEM. Statistical comparison was based on the Student t test or repeated measures two-way analysis of variance. A Spearman's rank correlation was used to determine the direction and strength of relationships between two different variables.

Results

Labeling DCs with Low Concentrations on MPIO has No Significant Effect on DC Viability

The aim of this study was to demonstrate that MPIO can be used as a MR contrast agent in order to monitor DC migration *in vivo* without affecting DC viability, phenotype, or function. Since this was the first study investigating the

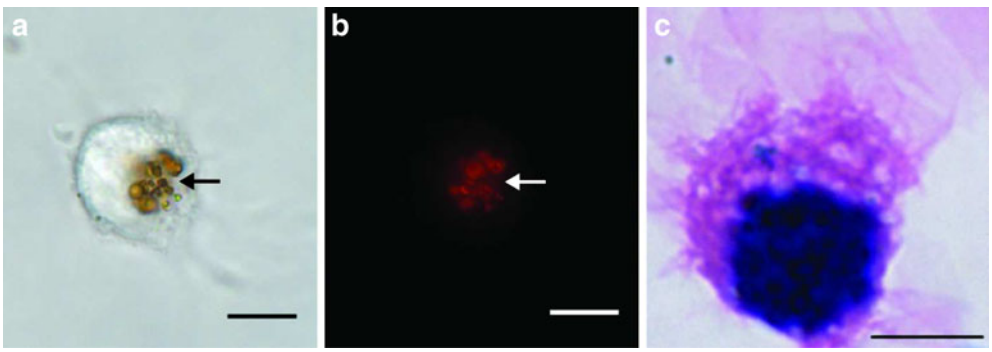

Fig. 1. Bone marrow-derived mouse DC efficiently uptake MPIO particles following overnight culture *in vitro.* DCs were labeled overnight with 12.5 µg/mL of MPIO, collected on day 5, and imaged using **a** bright-field microscopy or **b** fluorescence microscopy to detect the presence of intracellular MPIO particles. *Arrows* indicate the presence of MPIO particles. **c** DCs were alternatively stained with Perl's Prussian blue and counterstained with eosin to detect the presence of iron. Intracellular iron (*arrow*) was detected in the cytoplasm of MPIO-labeled DCs. Magnification = 100×, scale bar = 10 µm.

use of MPIO to label DCs, we needed to confirm that DCs were capable of taking up the particle in sufficient amounts to permit detection by cellular MRI. We show DCs readily take up MPIO *in vitro* following overnight culture, as depicted in Fig. 1. Specifically, we demonstrate that MPIO particles (brown) within the cytoplasm of DCs (Fig. 1a) correspond with red fluorescence from the Flash Red fluorophore-conjugated MPIO particles (Fig. 1b). Perl's Prussian blue staining showed that intracellular iron was detected in MPIO-labeled DCs (Fig. 1c).

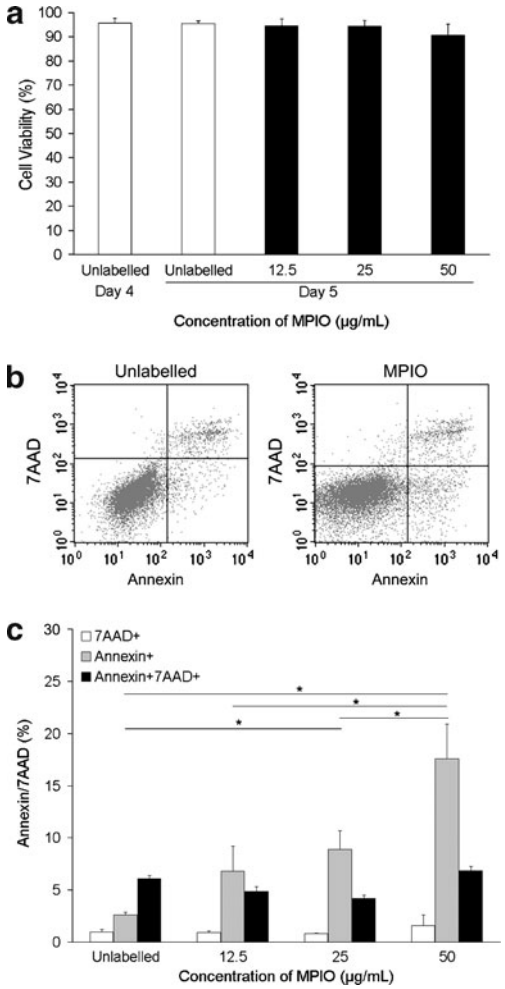

Fig. 2. Overnight labeling with low levels of MPIO particles does not affect viability or amount of apoptosis of DCs. **a** Viability of DCs as determined by the trypan blue exclusion assay was not affected following labeling with MPIO at any concentration. **b** Representative flow cytometry *dot plots* depicting 7AAD/Annexin staining of either unlabeled or MPIO-labeled (12.5 μg/mL) DCs. *Dot plots* are gated on $CD11c^+$ cells. **c** The percentage of DCs undergoing apoptosis ($Annexin^+$) was increased following labeling with MPIO at concentrations of 25 and 50 μg/mL compared to the unlabeled control. There were no changes in the percentage of cells that died due to necrosis ($7AAD^+$) or secondary apoptosis ($7AAD^+Annexin^+$).

In order to determine the percentage of DCs that take up MPIO particles following overnight incubation, magnetic column separation of MPIO-labeled cells from those that remained unlabeled was performed (de Chickera *et al*., submitted for publication). It was determined that following overnight incubation of DCs with MPIO nanoparticles, the MPIO labeling efficiency of DCs was 90%. It was also important to confirm that sufficient levels of iron were present within each cell so that they were detectable *in vivo* by MRI. The mean iron content in each cell was determined using ICP-MS and was found to be 12.5 pg of Fe/cell.

In order to determine any effects MPIO labeling itself might have on DCs, we assessed cellular viability following overnight culture of increasing concentrations (12.5, 25, and 50 μg/mL) of MPIO (Fig. 2). Cells were left unlabeled to serve as a control. The Trypan blue exclusion assay was used to assess DC viability, which remained unaffected by any concentration of MPIO (12.5, 25, and 50 μg/mL) following overnight labeling compared to unlabeled DCs (Fig. 2a). Annexin V/7AAD staining was used to investigate any effects MPIO labeling had on DC apoptosis or necrosis. Representative Annexin/7AAD flow cytometry dot plots for unlabeled (control) DCs and MPIO-labeled (12.5 μg/mL) DCs are shown (Fig. 2b). MPIO labeling at any concentration had no effect on the number of necrotic ($7AAD^+Annexin^-$) and secondary apoptotic cells ($7AAD^+Annexin^+$) DC (Fig. 2c) compared to the unlabeled control. However, the percentage of apoptotic cells increased following overnight incubation of both 25 and 50 μg/mL of MPIO tested compared to the unlabeled control. The increase in apoptotic cells was particularly pronounced at 50 μg/mL of MPIO. As a result, subsequent experiments carried out for this study employed the 12.5 μg/mL dose of MPIO, as it had the least affect on DC viability, apoptosis, or necrosis.

MPIO Labeling of DC has No Severe Effect on Phenotype or Function In Vitro

Ideally, MR contrast agents should label cells of interest for their subsequent detection *in vivo* by distinguishing them from surrounding tissues in an MR image without affecting either cellular phenotype or function. Therefore, it was important to confirm that labeling DCs with MPIO did not affect adversely their phenotype or function. Flow cytometric analysis of several surface markers important for DC maturation, Ag presentation and co-stimulation (CD80, CD86, MHCII, PD-1L, PD-2L), Ag uptake (CD36), activation and synapse formation (CD40, CD54), and migration (CD11c, CD11b, CCR7, CD38) was carried out on DCs labeled overnight with MPIO. Cells were left unlabeled to serve as an appropriate control (Fig. 3a). Overnight labeling of DCs with MPIO did not affect the mean fluorescence intensity or the percentage of positive cells for CD80, MHCII, PD-1l, PD-2L, CD54, CD11C, CD11b, CCR7, or CD38. Notably, however, MPIO labeling did induce DC

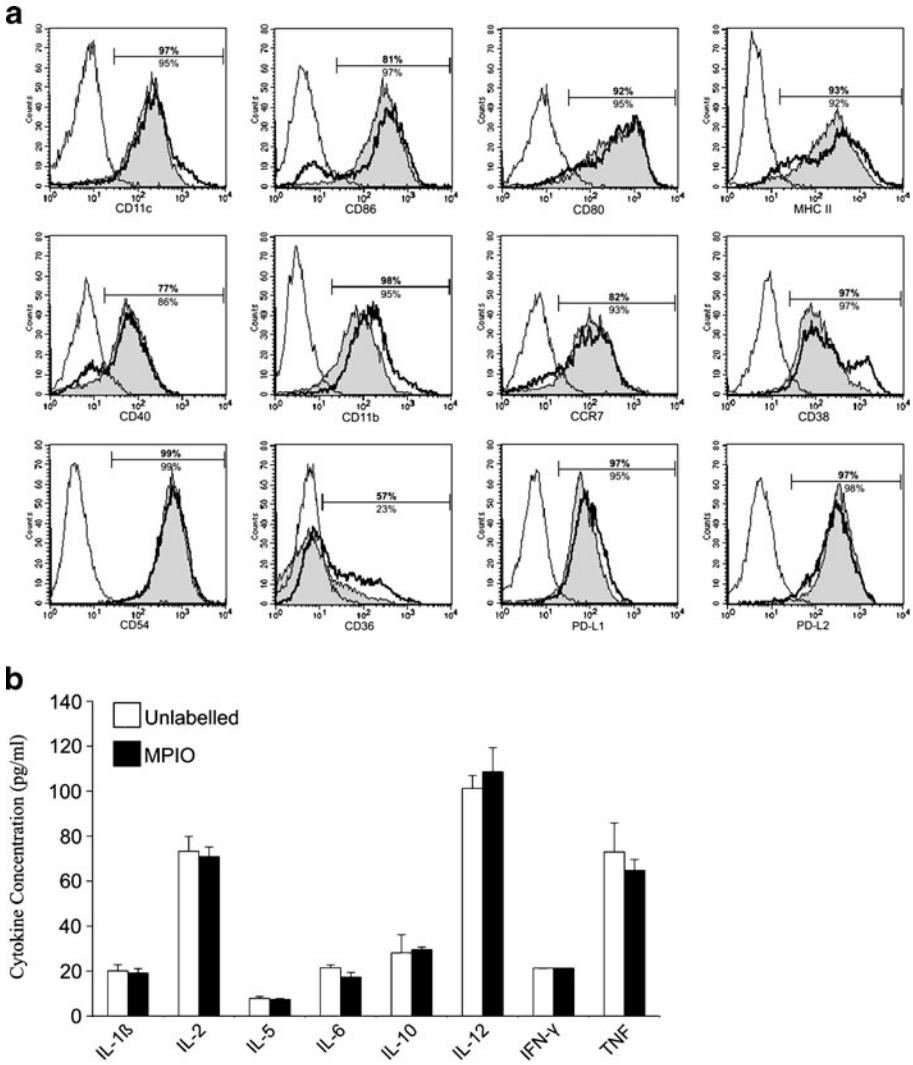

Fig. 3. Labeling BM-derived DC *in vitro* with MPIO affects their phenotype. **a** DCs were collected and stained for several phenotypic surface markers and analyzed using flow cytometry. MPIO labeling affects DC maturation (CD86) and DC activation (CD40) compared to the unlabeled control. MPIO labeling also causes a decrease in the percentage of $CD36^+$ DCs, a marker present on immature DCs. CD11c histogram is gated on viable cells, and all other histograms are gated on viable $CD11c^+$ cells. *Bold numbers* above histogram gates and numbers *below* histogram gates depict the percent of positive unlabeled and MPIO-labeled DCs, respectively. Histograms are representative of three independent experiments. **b** Supernatants from overnight MPIO-labeled DC cultures were collected, and Luminex assays were performed to determine the cytokine profiles. Supernatants collected from unlabeled DC cultures were used as a control. MPIO labeling does not significantly affect the cytokine profile of DCs ($P>0.05$). Data are the mean concentration (pg/mL) ± SE from three independent experiments.

maturation and activation *in vitro* as defined by CD86 and CD40 expression, respectively. The percentage of $CD11c^+CD86^+$ DC was significantly higher ($p<0.05$) for MPIO-labeled DCs (95.3±1.5%, $n=3$) compared to that of the unlabeled control DCs (80±1.7%, $n=3$). Similarly, the percentage of $CD11c^+CD40^+$ DC was also significantly higher ($p<0.05$) following overnight incubation with MPIO (75±10%, $n=3$) compared to that of unlabeled controls (66±10%, $n=3$). Coincident with the increase in DC maturation and activation, there was a significant 41% decrease ($p<0.05$) in number of DCs expressing CD36, a DC surface protein involved in apoptotic body uptake, a function normally expressed by immature DCs and downregulated as DC mature [27].

In addition to characterizing DC phenotype, *in vitro* functional cytokine profiles of DC cultures following overnight MPIO labeling were also analyzed. Supernatants were collected from *in vitro* MPIO-treated DC cultures; supernatants from DCs left unlabeled were used as controls. MPIO labeling of DCs had no affect on the secretion of mouse IL-1β, IL-2, IL-5, IL-6, IL-10, IL-12, TNF, or IFN-γ (Fig. 3b). When the functional cytokine analysis is considered along with the phenotypic analysis, the combined data indicate that MPIO had no adverse effects on DCs *in vitro*.

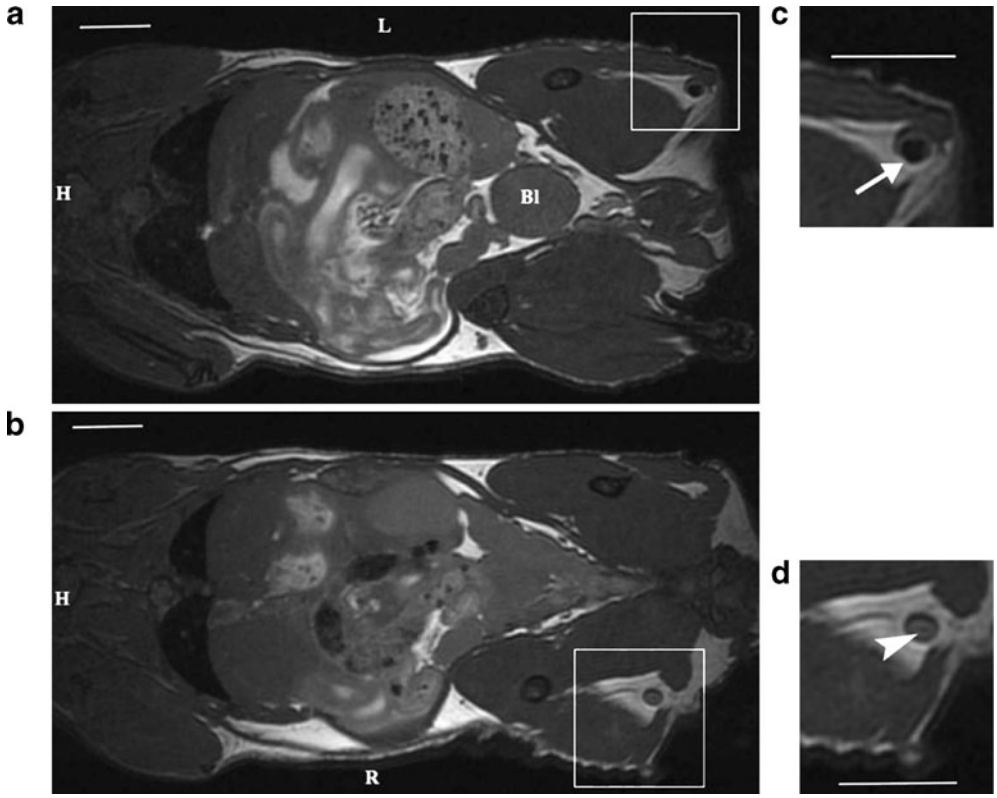

Fig. 4. Migration of DCs is detectable by cellular MRI. Coronal 3D-FIESTA images (200×200×200 μm) showing the popliteal lymph nodes from one representative mouse, 2 days after injection with **a** 1×10^6 MPIO-labeled DCs or **b** 1×10^6 unlabeled DCs. **c**, **d** *Cropped* and *enlarged* images of popliteal lymph nodes in **a** and **b** (*white boxes*). *Arrow* indicates the region of signal loss within the *left* lymph node and *arrowhead* points to signal loss due to the anatomical feature in the normal lymph nodes. *Bl* bladder, *H* head, *L* left, *R* right. Images are representative of $n=8$. Scale bar = 0.5 cm.

MPIO-Labeled DC can be Detected In Vivo by Cellular MRI

Although MPIO labeling induces DC maturation *in vitro* with respect to CD86 expression, the expression of surface proteins pertinent to DC migration (CCR7, CD38, and CD11b) remained unaffected. Therefore, we wanted to investigate any effect MPIO might have on the *in vivo* migration of DCs to target lymph nodes in a mouse model using cellular MRI. First, however, we had to determine if the MPIO-labeled DCs could be tracked *in vivo* using cellular MRI. Fig. 4 shows representative *in vivo* 3D-FIESTA coronal images of a mouse 2 days after injection of either 1×10^6 MPIO-labeled (Fig. 4a) or unlabeled DCs (Fig. 4b) into the left or right hind footpad, respectively. Cropped and enlarged images of the lymph nodes in Fig. 4a, b (white boxes) are shown in Fig. 4c, d, respectively. A distinct region of signal loss (arrow, Fig. 4c) was detectable in the left lymph node, while no signal loss was observed in the contralateral lymph node (Fig. 4d). Similar results were acquired for all mice imaged ($n=8$). The arrowhead in Fig. 4d points to an anatomical feature of the node that was observed in all nodes imaged which did not receive MPIO-labeled DC.

To determine if the region of signal loss in the draining lymph node is dose-dependent, two groups of mice ($n=8$/group) were injected with either 0.1 or 1.0×10^6 unlabeled (into right hind footpad) or MPIO-labeled DC (into left hind footpad). Fig. 5 shows representative *in vivo* 3D-FIESTA coronal images for mice pre-injection (Fig. 5a, c) and 2 days post-injection (Fig. 5b, d) of either 1×10^6 (Fig. 5a, b) or 0.1×10^6 MPIO-labeled DC (Fig. 5c, d). The region of signal loss encompassed most of the left lymph node following injection of 1×10^6 MPIO-labeled DC for all mice in this group ($n=8$). However, of the eight mice injected with 0.1×10^6 MPIO-labeled DCs, a region of negative signal loss was clearly detectable in the left popliteal lymph node of only one mouse (Fig. 5d).

The lymph node volumes were measured from MR images collected from all mice pre-injection and 2 days post-injection of unlabeled or MPIO-labeled DCs (Fig. 6). Data reveal that the volumes of popliteal lymph nodes increased significantly 2 days post-injection compared to pre-injection volumes (day 0) in all mice. The average volume of the normal lymph node at day 0 was 0.6 mm^3 ($n=16$), and the average lymph node volume at 2 days after the injection of 0.1×10^6 or 1×10^6 DC was approximately 1.2 and 2 mm^3, respectively. Furthermore, a dose-dependent increase in the lymph node volume was seen with respect to the number of DCs injected, as the lymph node volume from mice that received 1×10^6 DCs was greater than those that received

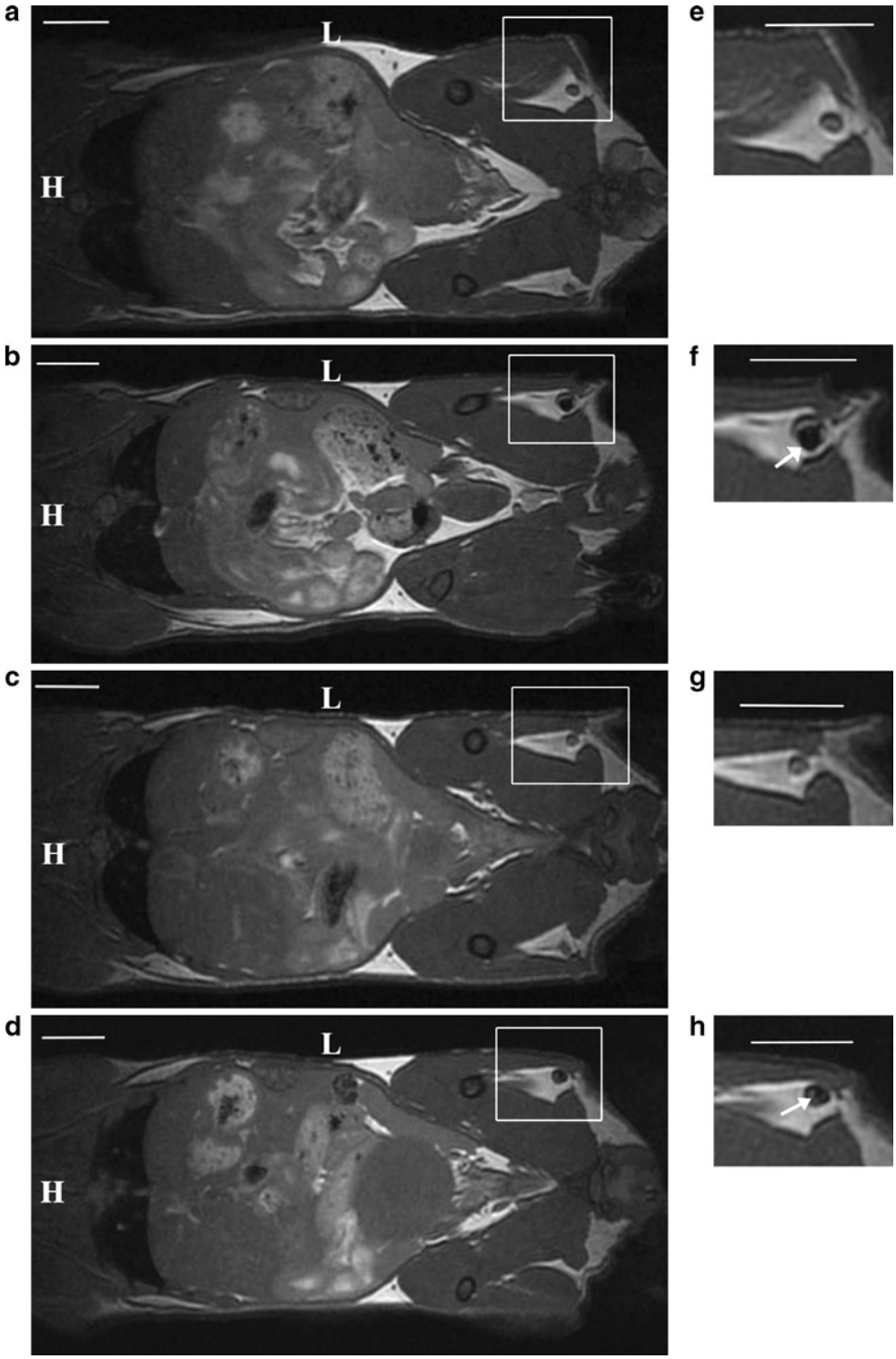

Fig. 5. Signal loss in MR images is different for different numbers of injected MPIO-labeled DCs. Coronal 3D-FIESTA images (200×200×200 μm) showing the popliteal lymph nodes from two representative mice **a** before and **b** 2 days after injection with 1×10^6 MPIO-labeled DCs or **c** before and 2 days **d** after injection with 0.1×10^6 MPIO-labeled DCs. **e**, **f**, **g**, **h** *Cropped* and *enlarged* images of popliteal lymph nodes in **a**, **b**, **c**, and **d** (*white boxes*), respectively. *Arrows* indicate the region of signal loss within the *left* lymph nodes. *Bl* bladder, *H* head, *L* left, *R* right. Images are representative of $n=16$; $n=8$ for each DC dose. Scale bar = 0.5 cm.

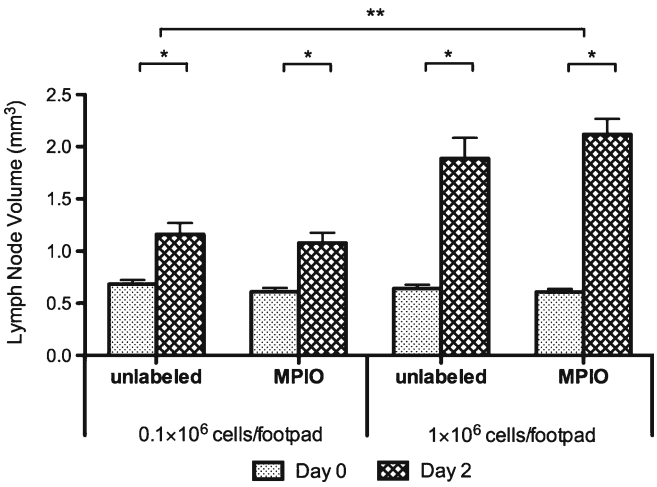

Fig. 6. Quantification of lymph node volume from images acquired at pre-injection and 2 days after DC injection. *Horizontal bars* represent mean values ± SEM ($n=8$ for each DC dose, $^{*}P<0.01$ day 2 vs. day 0, $^{**}P<0.001$ for 1×10^6 vs. 0.1×10^6 cells/footpad).

0.1×10^6 DCs on day 2 compared to day 0 (3.3- and 2-fold, respectively). The increases in lymph node volume following DC injection were not statistically different between mice injected with unlabeled DCs compared with MPIO-labeled DCs.

Next, we performed a time course experiment to determine if MPIO labeling of DCs affected the rate at which the cells migrated to popliteal lymph nodes. It has been determined that the peak amount of DC migration to a draining lymph node is 2 days post-injection [28, 29]. To see if the kinetics of MPIO-labeled DC migration to the popliteal lymph node is altered, mice were injected with either 0.1×10^6 or 1×10^6 MPIO-labeled or unlabeled DC into their left or right hind footpads, respectively. Mice were imaged using MRI at 2, 3, and 7 days post-injection. Fig. 7 shows cropped and enlarged images of the right (a) and left (b) popliteal lymph nodes for a representative mouse injected in the corresponding hind footpad with 1×10^6 unlabeled or MPIO-labeled DC. The region of signal loss within the left popliteal lymph node was evident at day 2 post-injection and appears to increase over time between days 2 and 7. This hypointense region encompassed a large extent of the left lymph node at all post-injection time points. Importantly, no signal loss was observed in any lymph nodes other than the popliteal lymph nodes following injection of either 0.1×10^6 or 1×10^6 MPIO-labeled DCs.

Fig. 8 shows results of the quantitative analysis of the MR images for the four mice imaged at days 2, 3, and 7 post-injection. The fractional signal loss and the signal void volume were only measured for the mice injected with 1×10^6 MPIO-labeled DCs because the signal void did not consistently appear in all mice injected with 0.1×10^6 MPIO-labeled DCs (two of four). The fractional signal loss measured in the popliteal lymph nodes following administration of 1×10^6 MPIO-labeled DCs was greatest on day 7 at 0.92 (Fig. 8a). Furthermore, the fractional signal loss at day 7 was significantly greater than that at day 2 but not day 3. Similarly, signal void volume increased over time following the injection of the 1×10^6 MPIO-labeled DCs (Fig. 8b). There is a significant difference between the signal void volume at day 2 (mean value of 0.933 mm^3) and day 3 (mean value of 1.22 mm^3) compared to day 0, as well as between days 3 and 7 (mean value of 2.30 mm^3). Quantification of the lymph node volume was also carried out, and data indicate that lymph node volumes increased over the 7-day imaging period (Fig. 8c). There was no difference in lymph node volumes between mice injected with labeled

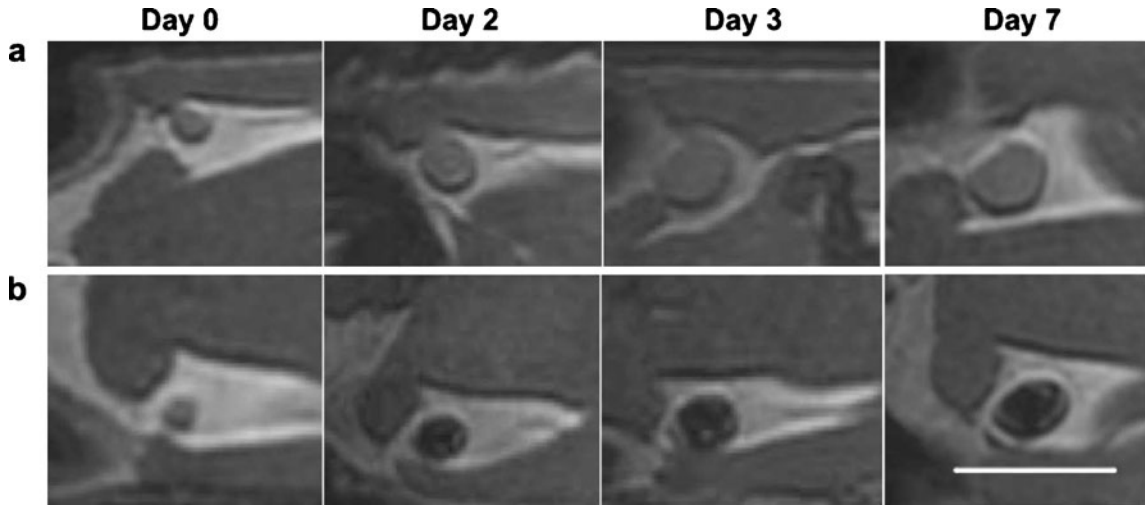

Fig. 7. Representative *in vivo* coronal images of popliteal lymph nodes at different time points after injection of 1×10^6 DCs. Coronal 3D-FIESTA images (*cropped* and *enlarged*) of the **a** *right* and **b** *left* popliteal lymph nodes at 72 h pre-injection and at days 2, 3, and 7 post-injection, after injection with **a** 1×10^6 unlabeled DCs or **b** 1×10^6 MPIO-labeled DCs. A region of hypointensity was detected at day 2 after injection and persisted up to day 7. Images are representative of $n=8$. Scale bar = 0.5 cm.

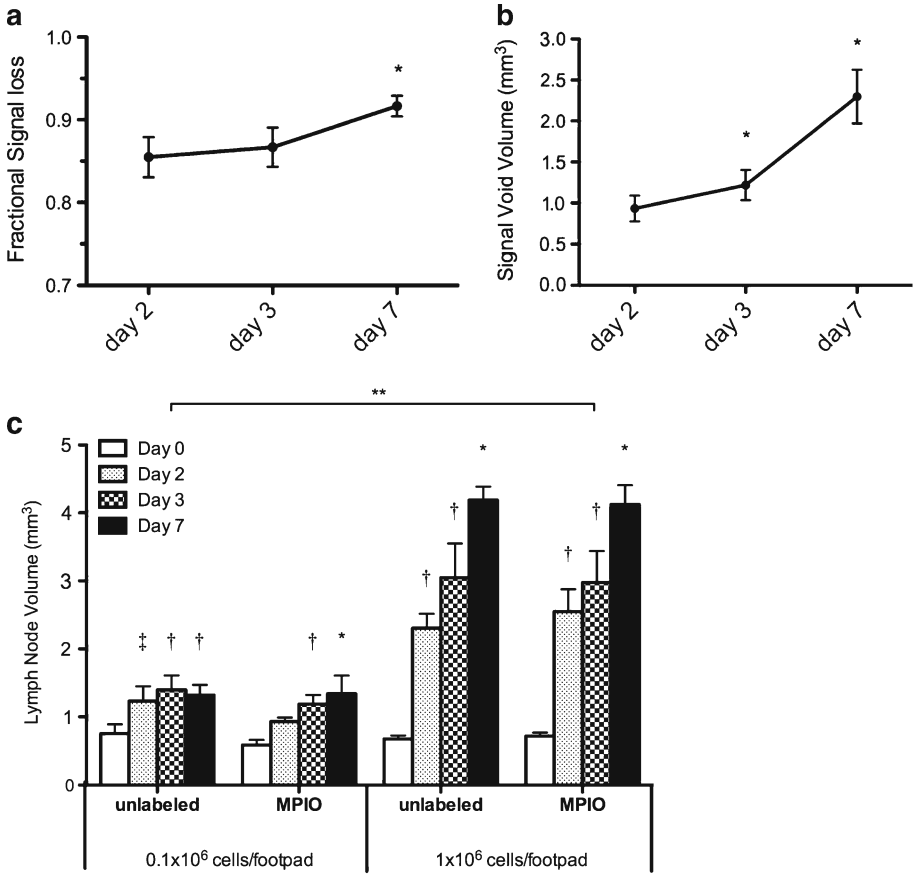

Fig. 8. Measurements of the lymph node volume, signal void volume, and the fractional signal loss. **a** Fractional signal loss and **b** signal void volume were measured from images acquired 2, 3, and 7 days after injection of 1×10^6 DCs. *Horizontal bars* represent mean values ± SEM (*$P<0.05$ for day 2 vs. day 3 and day 3 vs. day 7). **c** Lymph node volume was measured from images acquired pre-injection (day 0) and 2, 3, and 7 days post-injection. Data are means±SEM ($n=8$ for 1×10^6 cells/footpad and $n=4$ for 0.1×10^6 cells/footpad). Post-injection time points vs. day 0—‡$P<0.05$, †$P<0.01$, *$P<0.001$. **$P<0.01$ for 1×10^6 cells/footpad vs. 0.1×10^6 cells/footpad.

versus unlabeled DCs at any day. Again, a dose-dependent increase in the lymph node volume was observed; the volume of the popliteal nodes in mice that received 1×10^6 DCs was greater than the volume in mice that received 0.1×10^6 DCs at all time points.

MPIO Labeling Decreases DC Migration In Vivo

In order to confirm MRI results and determine any effect MPIO had on DC migration to the draining lymph node, conventional digital morphometry was carried out. To be able to detect either MPIO-labeled or unlabeled DCs in the lymph node using fluorescence microscopy, DCs were labeled with a green membrane linker dye, PKH67, prior to their injection. After MR imaging, mice were euthanized and popliteal lymph nodes were removed and processed for analysis of the area of $PKH67^+$ fluorescence using digital morphometry. Fig. 9 shows representative fluorescent images of popliteal lymph nodes from mice 2 days after receiving either 1×10^6 or 0.1×10^6 $PKH67^+$ MPIO-labeled DCs into the left hind footpad. Either 0.1×10^6 or 1×10^6 $PKH67^+$ unlabeled DCs were injected into the respective contralateral right hind footpads of the mice to serve as a control. $PKH67^+$ fluorescent unlabeled and MPIO-labeled DCs were detected mainly in the central areas of the lymph node cortex in all cases. The area of green PKH67 fluorescence was 8–10× greater following the injection of 1×10^6 DCs compared to injection of 0.1×10^6 DCs, as assessed by digital morphometry (Fig. 10a).

Of particular importance was the observation that the amount of PKH67 fluorescence in the draining lymph nodes was significantly greater in nodes from mice injected with unlabeled DCs (Fig. 10a). For mice injected with 0.1×10^6 DCs the area of green PKH67 was 1.9× greater for unlabeled DCs, and for mice injected with 1×10^6 DCs, the area of fluorescence was 2.4× greater for unlabeled DCs. This data suggests that the ability of MPIO-labeled DCs to migrate from the site of injection to the popliteal lymph nodes was impaired compared to unlabeled DCs.

The area of Flash Red fluorescence was also measured using digital morphometry in order to determine the percentage of DCs labeled with MPIO nanoparticles present

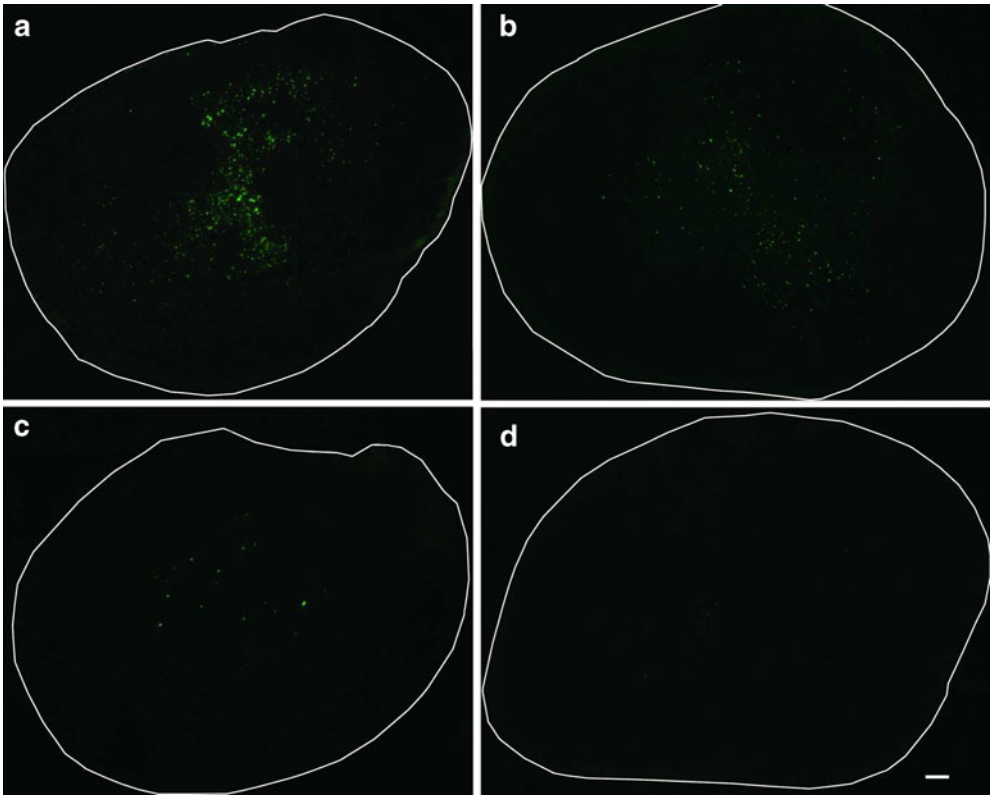

Fig. 9. Distribution of green PKH fluorescence in popliteal lymph nodes. Distribution of green PKH fluorescence in popliteal lymph nodes 2 days after injection of **a** 1×10^6 unlabeled DCs, **b** 1×10^6 MPIO-labeled DCs, **c** 0.1×10^6 unlabeled DCs, or **d** 0.1×10^6 MPIO-labeled DCs. The *green fluorescent regions* correspond to the presence of PKH^+ DC. Scale bar = 100 μm.

in the draining lymph nodes 2 days post-injection. Consistent with the PKH67 morphometric data, the area of MPIO-associated Flash Red^+ fluorescence was also significantly greater (ten-fold) after injection of 1×10^6 MPIO-labeled DCs compared with 0.1×10^6 MPIO-labeled DCs (Fig. 10b).

Within the same lymph node section, the distribution of $PKH67^+$ cells was very similar to the distribution of Flash Red MPIO particles at 2 days post-injection (Fig. 11a, b). A strong positive correlation between the amount of $PKH67^+$ fluorescence and the amount of Flash Red^+ fluorescence in the draining lymph nodes at day 2 was found (R^2=0.928, Fig. 11c).

Next, we assessed the distribution of $PKH67^+$ and Flash Red^+ fluorescent cells at day 7 in the popliteal lymph nodes. The pattern of PKH67 fluorescence observed in lymph nodes removed at day 7 post-injection was similar to that observed at day 2 post-injection. As observed at day 2 post-injection, the amount of PKH67 fluorescence at 7 days post-injection was greater after the injection of unlabeled DCs compared to MPIO-labeled DCs (2.7× greater). Another important observation was that the area of Flash Red fluorescence on day 7 was 2.3× greater than the area of green PKH67 fluorescence (Fig. 12). The level of PKH67 fluorescence was approximately 50% less in nodes examined at day 7 post-DC injection, compared to day 2, yet the level of Flash Red^+ fluorescence was not different (Figs. 10 and 12). This suggests that the cells that originally contained MPIO do not persist as long as the MPIO particles themselves within the lymph node.

Discussion

There have been a number of studies which used cellular MRI to track iron-labeled DCs *in vivo*. One cell tracking study used ultra-small SPIO (USPIO) particles to label mouse DC [13]. In this study, USPIO-labeled DCs were detected at the site of injection after intramuscular administration in spin-echo images on a 11.7 T MRI scanner. However, no DCs were detected in the draining lymph nodes. A few groups have reported the use of SPIO nanoparticles to label and track DCs *in vitro* and *in vivo* [10–15]. Specifically, three groups have demonstrated that the migration of SPIO-labeled DCs to draining lymph nodes in mice can be detected using cellular MRI [12, 14, 15]. Baumjohann *et al*. were first to demonstrate this in 2006 using SPIO-labeled DCs in mice imaged at 4.7 T [15]. SPIO nanoparticles have also been used to label human DCs [10], which were subsequently administered via intranodal injection to melanoma patients under ultrasound guidance. Imaging was performed using a gradient echo sequence on a 3 T clinical MRI scanner. MRI allowed for the assessment of accuracy of intranodal DC administration as well as the visualization of the migration of DCs between adjacent or

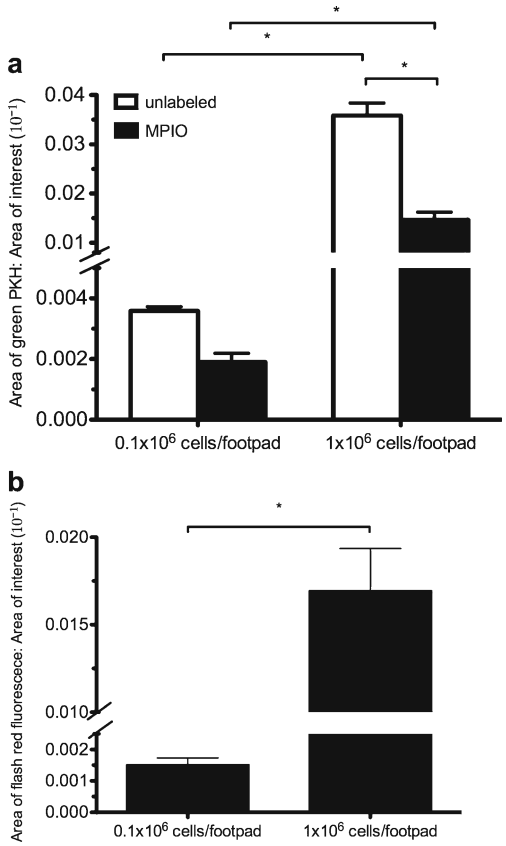

Fig. 10. Measurements of the area of fluorescence in popliteal lymph nodes 2 days post-injection. **a** The area of green PKH fluorescence and **b** Flash Red fluorescence were measured by digital morphometry. Data are mean± SEM ($n=4$ per group, $^*P<0.05$).

paired nodes. Recently, we demonstrated that migration of SPIO-labeled DCs can be tracked *in vivo* in a mouse model using the FIESTA pulse sequence on 1.5 T clinical scanner [12]. In that study, we presented a semi-quantitative approach to assess the amount of DC migration to popliteal lymph nodes using MRI and demonstrated a positive correlation between the fractional signal loss from MR image data and conventional histological analysis.

SPIO nanoparticles have been the MR contrast agent of choice for tracking DC migration *in vivo* using cellular MRI. This study, however, presents the first report of tracking of MPIO-labeled DC *in vivo* using cellular MRI. Using custom MRI equipment and an acquisition protocol previously optimized by our group for the *in vivo* detection of iron-labeled cells, such as SPIO-DC, we were able to detect MPIO-labeled DCs *in vivo* using cellular MRI [12, 22, 30, 31]. The system includes a custom-built, high-performance gradient coil insert used with a clinical 1.5 or 3 T MRI scanner running the 3D-FIESTA (fast imaging employing steady-state acquisition) pulse sequence with RF phase cycling. The FIESTA pulse sequence provides high signal-to-noise ratio in short scan times and is very insensitive to the effects of iron particles. The combination of this MRI system and protocol has allowed us to acquire images with high signal-to-noise ratio and sensitivity, giving us the ability to image the whole mouse body while simultaneously imaging distinct regions of signal loss due to MR contrast-labeled cells in lymph nodes in less than 25 min.

Previously, MPIO have been used for the detection of cancer cells, T cells, macrophages, and stem cells in preclinical animal models [20–23, 32–34]. In general, however, MPIO is used less often as an MR contrast agent in comparison to SPIO for cell tracking studies. When compared to SPIO nanoparticles, MPIO particles differ with respect to size, amount of iron per particle, and surface coating. MPIO particles are the largest of the iron-based MR contrast agents and contain, on average, the most amount of iron per particle. Therefore, as the presence of several SPIO nanoparticles may be necessary for the detection of a single cell by cellular MRI, the higher iron content of MPIO enables the detection of a cell containing even a single MPIO particle [32]. One critically relevant factor when comparing the use of MPIO and SPIO nanoparticles for tracking DC migration using MRI is the surface chemistry of each MR agent. Generally, iron-based MR contrast agents are coated with a polymer to prevent their immediate degradation *in vivo*. MPIO is coated with an inert, and therefore, non-biodegradable, polystyrene coat, while SPIO is covered in dextran, rendering it biodegradable [18]. The biologically inert polystyrene coat renders MPIO particles more resistant to degradation *in vivo*, especially when compared to SPIO nanoparticles. As a result, MPIO nanoparticles potentially have the ability to persist *in vivo* for longer periods of time [18].

In order to label our DCs with MPIO particles *in vitro*, simple co-incubation of DCs with MPIO overnight was sufficient. We did not require the addition of either polycationic agents or lipid-based reagents, largely due to the inherent endocytic abilities of DC. Compared to our previously published results with SPIO [12], MPIO-labeled DC contained 3–4× more iron per cell (12.5 pg of Fe/cell). Furthermore, *in vitro* labeling of DC with MPIO particles was more efficient (90%) compared to that of SPIO nanoparticles (75–86%, de Chickera *et al*., submitted for publication). Viability of labeled DCs was not significantly affected at the lower range of MPIO concentrations tested (12.5–25 μg/mL). While labeling DCs with MPIO did not affect the majority of the cell surface markers of DC function, MPIO did affect the number of DCs expressing CD86 and CD40, important markers of mouse DC maturation and activation, respectively. Overnight incubation of DCs with MPIO resulted in a more uniform population of mature $CD11c^+CD86^+$ DCs, where the comparable unlabeled control DCs were a 80–20% mixture of mature and immature ($CD11c^+CD86^-$) DCs. The DC activation marker, CD40, followed a similar trend. Of note is that this MPIO-induced maturation and activation occurred in the absence of any pro-inflammatory cytokines and/or activation agonists

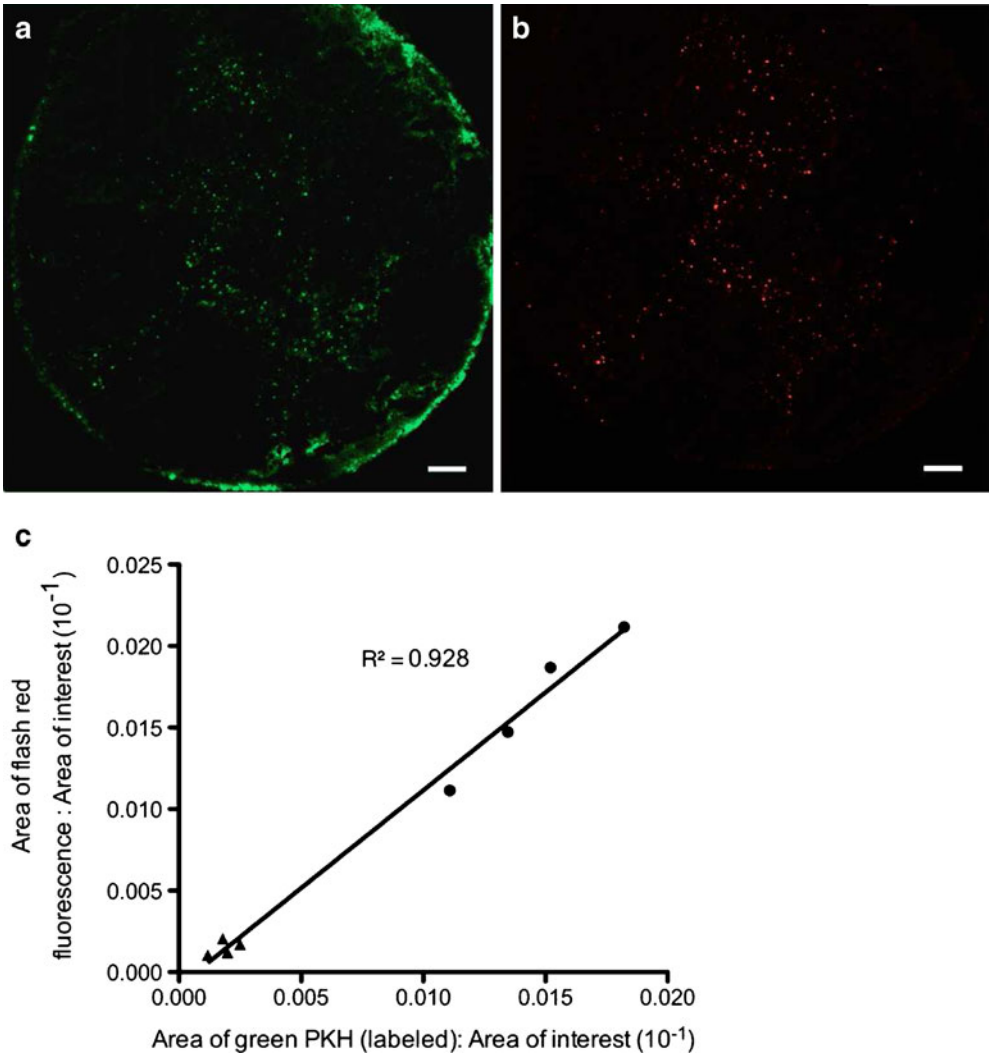

Fig. 11. Distribution of green PKH$^+$ DC and Flash Red MPIO in popliteal lymph nodes 2 days after the injection of DCs. **a** The distribution of green PKH$^+$ DC is consistent with **b** the distribution of flash red MPIO particles. **c** There is a strong positive correlation between amount of green PKH fluorescence and amount of Flash Red fluorescence in the left lymph node (R^2 = 0.928; *filled triangle* indicates data point for 0.1×10^6 cells/footpad; *filled circle* indicates data point for 1×10^6 cells/footpad). The *green fluorescent regions* correspond to the presence of PKH$^+$ DC and the *red fluorescent regions* correspond to the presence of MPIO particles. Scale bar = 100 μm.

normally used to mature and activate DCs prior to injection [35]. Coincident with the increased percentage of mature DCs was a reduction in percentage of CD11c$^+$CD36$^+$ DC, which is involved in the endocytosis of apoptotic bodies. This is not surprising because as DCs mature they lose their ability to endocytose and increase their ability to migrate and present Ag [27]. However, we cannot rule out that the uptake of MPIO directly leads to the reduction in DC surface expressed CD36. Alternatively, MPIO uptake may have resulted in a combination of maturation-induced reduction in CD36 surface expression and surface desensitization and internalization of CD36.

In vivo, mature, and activated DCs are highly competent for migration compared to immature DCs. It follows, then, that because MPIO labeling produced a more mature population of DCs, more MPIO-labeled DCs should migrate to the lymph nodes following injection into mice compared to unlabeled DCs. However, when migration was compared between MPIO-labeled and unlabeled DCs, data indicated that there was a significant reduction in the migration of MPIO-labeled DCs compared to unlabeled DCs. This same observation has been made with SPIO-labeled DC [12]. Our *in vitro* assays of cell viability did not reveal substantial negative effects of labeling with MPIO, so viability could not be a factor that is impeding the *in vivo* migration of these DCs. *In vitro* and *in vivo* studies from our group indicate that in the mouse, SPIO and MPIO particles are most likely physically impeding the migration of DCs through the reticuloendothelial cell junctions (de Chickera *et al*., submitted for publication).

In mice injected with 1×10^6 MPIO-labeled DCs an obvious region of signal void was present in the popliteal

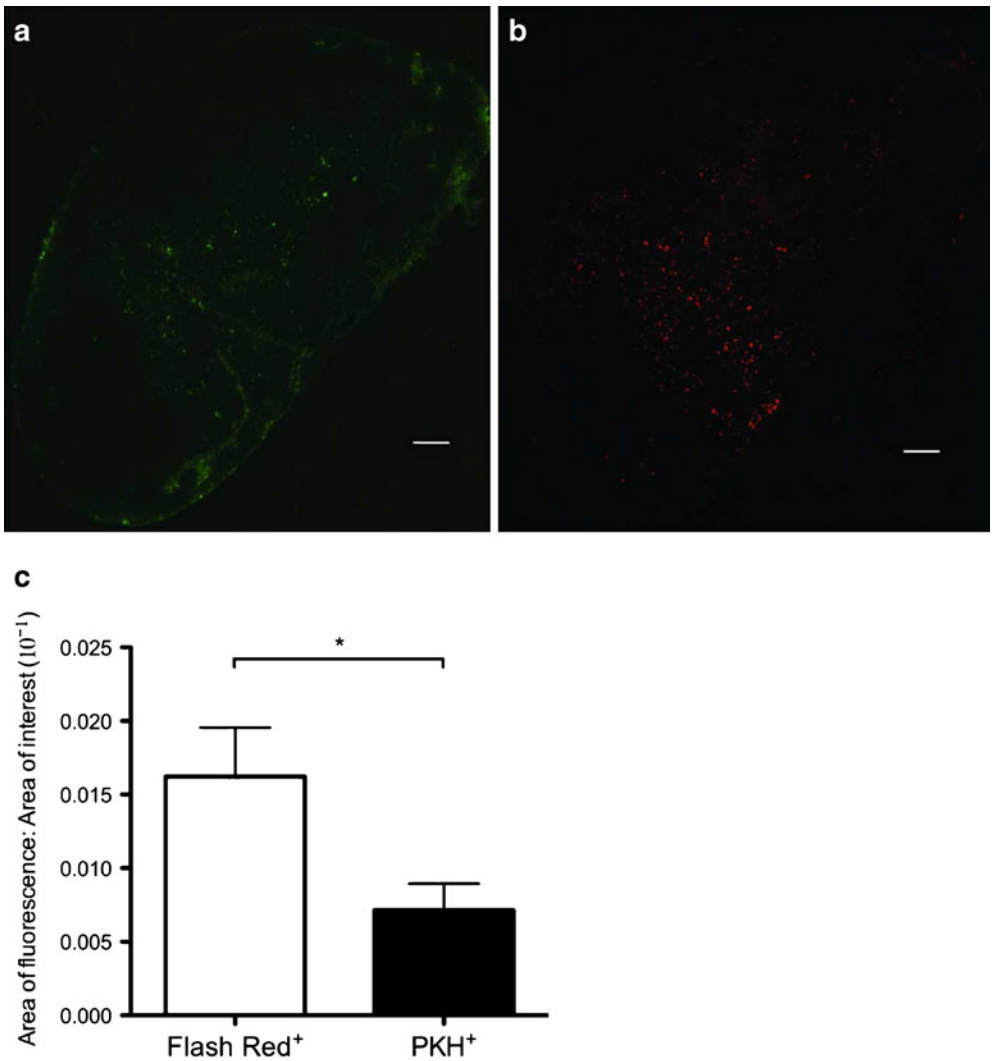

Fig. 12. Distribution of green PKH$^+$ DC and flash red MPIO in popliteal lymph nodes 7 days after the injection of 1×10^6 MPIO-labeled DCs. The areas of **a** green PKH fluorescence and **b** flash red fluorescence were measured by digital morphometry. **c** The area of Flash Red fluorescence on day 7 was 2.3× greater than the area of green PKH67 fluorescence ($n=4$ per group, $^*P<0.05$). The *green fluorescent regions* correspond with the presence of PKH$^+$ DCs and the *red fluorescence regions* correspond to the presence of MPIO particles. Scale bar = 100 μm.

lymph nodes of all mice. The analysis of MR images revealed an increase in the volume of the lymph node after the injection of DCs. This was true whether MPIO-labeled or unlabeled DCs were injected. This seems to contradict the finding of a reduction in the migration of MPIO-labeled DCs compared to unlabeled DCs. The increased node volume is the result of an increase in lymph node cellularity, mainly due to proliferation of T cells, triggered by the presence of DCs in the node. The relationship between the numbers of DCs injected and the increase in node cellularity is, however, not linear [8]. In addition, a small number of DCs may stimulate a large number of T cells. It has been reported that only one DC is necessary to turn on 100–3,000 T cells [36]. There is also a threshold level of DCs required to enter the node to result in T cell proliferation and a maximal number of DCs that can enter the node [37]. Therefore, the most likely explanation for this discrepancy is that different numbers of DCs migrating to the lymph node (providing the threshold is reached) can result in similar levels of cell proliferation.

Currently, an advantageous feature of MPIO particles is the availability of fluorescently tagged MPIO particles. These tags, which are available in a variety of fluorescent dyes, facilitate the direct detection of MPIO particles present within cells or tissues using fluorescence microscopy. Thus, fluorescently tagged MPIO particles provide some advantages in terms of application in comparison to SPIO nanoparticles. The Flash Red-conjugated MPIO particles used in this study enabled the direct visualization of iron particles in the lymph nodes using fluorescent microscopy, thereby allowing for comparisons between the presence and location of MPIO and DCs labeled with PKH67.

Digital morphometric analysis of the PKH67$^+$ cells and Flash Red (MPIO) fluorescence in this experiment was

designed to investigate whether signal loss in the draining lymph node MR images truly reflected the presence DC (PKH^+) in the draining lymph node. It has been suggested that the number of DC in draining lymph nodes peaks 48 h following subcutaneous injection, and this number subsequently declines naturally by apoptosis due to the lifespan of mature and activated DCs [28, 29]. Our imaging results with MPIO-labeled DCs show that signal loss is present in the nodes at day 2 post-injection. However, this signal loss persists, and actually increases in the same nodes, over 7 days post-injection. This MRI result is in agreement with our recent work which demonstrated that the signal loss associated with SPIO-labeled DC also persists for 7 days; although for SPIO the extent of signal loss peaks at day 2 and subsequently decreases on days 3, 4, and 7 post-DC injection (de Chickera *et al*., submitted for publication).

The MRI observations for MPIO are, however, in contrast to what was observed by digital morphometry. The extent of $PKH67^+$ fluorescence was ~50% less at day 7 compared to day 2 and was less than the extent of Flash Red fluorescence at day 7. The level of Flash Red^+ fluorescence however remained relatively constant when comparing days 2 and 7. There are a few things that may explain these findings. First, as the migrated DCs die in the node they may release their MPIO content, which can be ingested and retained by resident lymph node DCs and macrophages. This likely explains the persistence of signal loss beyond the lifespan of DCs.

Second, MPIO may be transported to the lymph node more slowly than expected and therefore iron may accumulate in the node with time. If this is true then the MPIO must be brought to the draining lymph node by endogenous recipient DCs or macrophages as the $PKH67^+$ content did not increase in parallel with the observed MRI detected signal loss. A previous study on *in vivo* SPIO labeling and tracking of endogenous DC showed that endogenous DC capture SPIO released from injected dying tumor cells and migrate to lymph nodes [14]. This may explain the disparity in the amount of green PKH67 and red MPIO fluorescence at day 7.

Finally, the size of the region of signal loss (also called the blooming artifact) depends on the amount of iron present, the imaging parameters, and also on how the total iron concentration per voxel is distributed in a tissue. Because the volume of the lymph node is increasing with time, the iron concentration per voxel is changing as well. So the same amount of iron, redistributed in the node tissue, may appear as a larger area of signal void. This may explain the increasing amount of signal loss in the MR images. It is likely that all of these explanations are relevant to the interpretation of our observations at day 7 post-DC injection.

Ultimately, while this study and previous studies from our group have demonstrated that both MPIO and SPIO can be used to successfully track the migration of DCs to a draining lymph node, the choice of which to use will depend on the question being asked. If the objective is to examine DC migration, then SPIO may provide a more accurate assessment. If the objective is to identify the site(s) to which DCs migrate, then MPIO particles may be more appropriate.

Conclusion

This paper presents the first report of the successful use of fluorescent MPIO particles to track DC migration. The observations of these experiments indicate that MPIO-labeled DCs can be reliably tracked *in vivo* by MRI in the short term and therefore will be useful for imaging small numbers of cells in preclinical investigations. The interpretation of signal loss in images of MPIO-labeled DCs at time points longer than the lifespan of DCs is complicated and needs to be done with caution.

Acknowledgments. This research was supported by grants from the Ontario Institute for Cancer Research and the Terry Fox Foundation for Cancer Research. Sonali de Chickera was supported by the Frederick Banting and Charles Best Canada Graduate Scholarship Master's Award (CIHR) and the Translational Breast Cancer Research Trainee Studentship (London Health Sciences Centre). We would like to thank Dr. Renata Raina for her technical assistance with the ICP-MS analysis. Her work was carried out at the Trace Analysis Facility at the University of Regina, Regina, Saskatchewan, Canada, which was supported by a Canadian Foundation for Innovation. We would also like to thank Mia Merrill for her assistance in making some figures for this manuscript. We also acknowledge Drs. Brian Rutt and Andrew Alejski for the design and construction of the MR hardware.

Conflict of Interest Disclosure. The authors declare that they have no conflict of interest.

References

1. Perales MA, Yuan J, Powel S et al (2008) Phase I/II study of GM-CSF DNA as an adjuvant for a multipeptide cancer vaccine in patients with advanced melanoma. Mol Ther 16:2022–2029
2. Disis ML, Grabstein KH, Sleath PR et al (1999) Generation of immunity to the HER-2/neu oncogenic protein in patients with breast and ovarian cancer using a peptide-based vaccine. Clin Cancer Res 5:1289–1297
3. Farkas A, Conrad C, Tonel G et al (2006) Current state and perspectives of dendritic cell vaccination in cancer immunotherapy. Skin Pharmacol Physiol 19:124–131
4. Thurner B, Haendle I, Röder C et al (1999) Vaccination with mage-3A1 peptide-pulsed mature, monocyte-derived dendritic cells expands specific cytotoxic T cells and induces regression of some metastases in advanced stage IV melanoma. J Exp Med 190:1669–1678
5. Ridgway D (2003) The first 1000 dendritic cell vaccines. Cancer Investig 21:873–886
6. Steinman RM, Banchereau J (2007) Taking dendritic cells into medicine. Nature 449:419–426
7. Aarntzen EH, Figdor CG, Adema GJ et al (2008) Dendritic cell vaccination and immune monitoring. Cancer Immunol Immunother 57:1559–1568
8. Martin-Fontecha A, Sebastiani S, Höpken UE et al (2003) Regulation of dendritic cell migration to the draining lymph node: impact on T lymphocyte traffic and priming. J Exp Med 198:615–621
9. de Vries IJ, Krooshoop DJ, Scharenborg NM et al (2003) Effective migration of antigen-pulsed dendritic cells to lymph nodes in melanoma patients is determined by their maturation state. Cancer Res 63:12–17
10. de Vries IJ, Lesterhuis WJ, Barentsz JO et al (2005) Magnetic resonance tracking of dendritic cells in melanoma patients for monitoring of cellular therapy. Nat Biotechnol 23:1407–1413
11. Verdijk P, Scheenen TW, Lesterhuis WJ et al (2006) Sensitivity of magnetic resonance imaging of dendritic cells for *in vivo* tracking of cellular cancer vaccines. Int J Cancer 120:978–984

12. Dekaban GA, Snir J, Shrum B et al (2009) Semiquantitation of mouse dendritic cell migration *in vivo* using cellular MRI. J Immunother 32:240–251
13. Ahrens ET, Feili-Hariri M, Xu H et al (2003) Receptor-mediated endocytosis of iron-oxide particles provides efficient labeling of dendritic cells for *in vivo* MR imaging. Magn Reson Med 49:1006–1013
14. Long CM, van Laarhoven HW, Bulte JW, Levitsky HI (2009) Magneto-vaccination as a novel method to assess and quantify dendritic cell tumor antigen capture and delivery to lymph nodes. Cancer Res 69:3180–3187
15. Baumjohann D, Hess A, Budinsky L et al (2006) *In vivo* magnetic resonance imaging of dendritic cell migration into the draining lymph nodes of mice. Eur J Immunol 36:2544–2555
16. Heyn C, Bowen CV, Rutt BK, Foster PJ (2005) Detection threshold of single SPIO-labeled cells with FIESTA. Magn Reson Med 53:312–320
17. Foster-Gareau P, Heyn C, Alejski A, Rutt BK (2003) Imaging single mammalian cells with a 1.5 T clinical MRI scanner. Magn Reson Med 49:968–971
18. Shapiro EM, Skrtic S, Koretsky AP (2005) Sizing it up: cellular MRI using micron-sized iron oxide particles. Magn Reson Med 53:329–338
19. Williams JB, Ye Q, Hitchens TK et al (2007) MRI detection of macrophages labeled using micrometer-sized iron oxide particles. J Magn Reson Imaging 25:1210–1218
20. Foley LM, Hitchens TK, Ho C et al (2009) Magnetic resonance imaging assessment of macrophage accumulation in mouse brain after experimental traumatic brain injury. J Neurotrauma 26:1509–1519
21. Shapiro EM, Medford-Davis LN, Fahmy TM et al (2007) Antibody-mediated cell labeling of peripheral T cells with micron-sized iron oxide particles (MPIOs) allows single cell detection by MRI. Contrast Media Mol Imaging 2:147–153
22. Bernas LM, Foster PJ, Rutt BK (2007) Magnetic resonance imaging of *in vitro* glioma cell invasion. J Neurosurg 106:306–313
23. Hinds KA, Hill JM, Shapiro EM et al (2003) Highly efficient endosomal labeling of progenitor and stem cells with large magnetic particles allows magnetic resonance imaging of single cells. Blood 102:867–872
24. de Vries IJ, Lesterhuis WJ, Scharenborg NM et al (2003) Maturation of dendritic cells is a prerequisite for inducing immune responses in advanced melanoma patients. Clin Cancer Res 9:5091–5100
25. Vanhoe H, Vandecasteele C, Versieck J, Dams R (1989) Determination of iron, cobalt, zinc, rubidium, molybdenum, and cesium in human serum by inductively coupled plasma mass spectrometry. Anal Chem 61:1851–1857
26. Saville LR, Pospisil CH, Mawhinney LA et al (2004) A monoclonal antibody to CD11d reduces the inflammatory infiltrate into the injured spinal cord: a potential neuroprotective treatment. J Neuroimmunol 156:42–57
27. Ardavín C, Martínez del Hoyo G, Martín P et al (2001) Origin and differentiation of dendritic cells. Trends Immunol 22:691–700
28. Huck SP, Tang SC, Andrew KA, Yang J, Harper JL, Ronchese F (2008) Activation and route of administration both determine the ability of bone marrow-derived dendritic cells to accumulate in secondary lymphoid organs and prime CD8+ T cells against tumors. Cancer Immunol Immunother 57:63–71
29. Hou WS, Van Parijs L (2004) A Bcl-2-dependent molecular timer regulates the lifespan and immunogenicity of dendritic cells. Nat Immunol 5:583–589
30. Heyn C, Ronald JA, Mackenzie LT et al (2006) *In vivo* magnetic resonance imaging of single cells in mouse brain with optical validation. Magn Reson Med 55:23–29
31. Gonzalez-Lara LE, Xu X, Hofstetrova K et al (2009) *In vivo* magnetic resonance imaging of spinal cord injury in the mouse. J Neurotrauma 26:753–762
32. Shapiro EM, Skrtic S, Sharer K et al (2004) MRI detection of single particles for cellular imaging. Proc Natl Acad Sci USA 101:10901–10906
33. Heyn C, Ronald JA, Ramadan SS et al (2006) *In vivo* MRI of cancer cell fate at the single cell level in a mouse model of breast cancer metastasis to the brain. Magn Reson Med 56:1001–1010
34. Ye Q, Wu YL, Foley LM et al (2008) Longitudinal tracking of recipient macrophages in a rat chronic cardiac allograft rejection model with noninvasive MRI with micron-sized paramagnetic iron oxide particles. Circulation 118:149–156
35. Urban BC, Willcox N, Roberts DJ (2001) A role for CD36 in the regulation of dendritic cell function. Proc Natl Acad Sci USA 98:8750–8755
36. Banchereau J, Steinman RM (1998) Dendritic cells and the control of immunity. Nature 392:245–252
37. Mempel TR, Henrickson SE, Von Andrian UH (2004) T-cell priming by dendritic cells in lymph nodes occurs in three distinct phases. Nature 427:154–159